Quaternary Science Reviews 28 (2009) 399–411 No. 5-6

Contents lists available at ScienceDirect

Quaternary Science Reviews

journal homepage: www.elsevier.com/locate/quascirev

Trends, rhythms and events in Plio-Pleistocene African climate

Martin H. Trauth [a,*], Juan C. Larrasoaña [b], Manfred Mudelsee [c]

[a] Institut für Geowissenschaften, Universität Potsdam, Karl-Liebknecht-Str. 24, 14476 Potsdam, Germany
[b] Institute of Earth Sciences Jaume Almera, CSIC, Solé i Sabaris s/n, Barcelona 08028, Spain
[c] Climate Risk Analysis, Schneiderberg 26, 30167 Hannover, Germany

ARTICLE INFO

Article history:
Received 18 July 2008
Received in revised form
21 October 2008
Accepted 10 November 2008

ABSTRACT

We analyzed published records of terrigenous dust flux from marine sediments off subtropical West Africa, the eastern Mediterranean Sea, and the Arabian Sea, and lake records from East Africa using statistical methods to detect trends, rhythms and events in Plio-Pleistocene African climate. The critical reassessment of the environmental significance of dust flux and lake records removes the apparent inconsistencies between marine vs. terrestrial records of African climate variability. Based on these results, major steps in mammalian and hominin evolution occurred during episodes of a wetter, but highly variable climate largely controlled by orbitally induced insolation changes in the low latitudes.

1. Introduction

Comparisons of marine and terrestrial paleoclimate archives have resulted in contrasting views on high- vs. low-latitude forcing of East Africa's climate and its role in mammalian and hominin evolution (deMenocal, 1995, 2004; Trauth et al., 2005, 2007; Maslin and Christensen, 2007). Marine records of Saharan dust suggest that major events in mammalian and hominin evolution were mediated by shifts towards more arid and variable conditions during the onset and amplification of high-latitude glacial cycles at 2.8 (±0.2) Ma, 1.7 (±0.1) Ma, and 1.0 (±0.2) Ma, which were superimposed on a regime of subdued moisture availability (deMenocal, 1995, 2004). On the contrary, the chronology of Plio-Pleistocene lake-level variations in East Africa suggest that these and other periods were characterized by the occurrence of large, but fluctuating lakes indicating consistency in wetter and more seasonal conditions (Trauth et al., 2005, 2007). According to this concept, mammalian and hominin species seem to differentially originate and go extinct during periods of extreme climate variability on high moisture levels controlled largely by low-latitude solar heating, rather than by high-latitude ice volume variations (Trauth et al., 2007).

Crucial to any discussion of contrasting views of climate changes and its role in evolution is the correct assessment and unambiguous interpretation of paleoclimatic data contained in marine vs. terrestrial archives. To date, marine dust records are the only type of record that enable the study of Plio-Pleistocene African climate at a large range of timescales (10^6–10^3 years) (Tiedemann et al., 1994; deMenocal, 1995, 2004; Larrasoaña et al., 2003). However, the evidence for a link between Saharo-Arabian dust deposition and changes of the mammalian and hominin habitats in Sub-Saharan Africa has not yet been substantiated. Unlike marine paleoclimate records, terrestrial records provide a more pristine view of environmental changes in East Africa, but fluctuating sedimentation rates combined with large dating errors in short and discontinuous records often hamper the correlation of environmental changes through time and space (Trauth et al., 2005, 2007).

Since long-term trends, shifts in the variability and abrupt transitions in African climates may have provided a catalyst for evolutionary changes, we statistically evaluate the significance of trends, rhythms and events in records of Plio-Pleistocene environmental changes. We analyzed three representative long marine dust flux records off subtropical West Africa, the eastern Mediterranean Sea, and the Arabian Sea and one representative record of global ice volume changes. Subsequently, we compared the results of our analysis with terrestrial records of Plio-Pleistocene African climate. The results of this analysis help better understand the processes changing the habitat of mammals and hominins and therefore provide a new basis for the discussion of climate–evolution linkages.

2. Proxy records for Plio-Pleistocene African climate

In this study, we analyzed three published records of terrigenous dust flux from marine sediments from the Arabian Sea (deMenocal et al., 1991; deMenocal, 1995, 2004), the eastern Mediterranean Sea (Larrasoaña et al., 2003) and off subtropical West Africa (Tiedemann et al., 1994) using statistical methods to

* Corresponding author. Tel.: +49 331 977 5810; fax: +49 331 977 5700.
E-mail address: trauth@geo.uni-potsdam.de (M.H. Trauth).

0277-3791/$ – see front matter © 2008 Elsevier Ltd. All rights reserved.
doi:10.1016/j.quascirev.2008.11.003

detect trends, rhythms and events in Plio-Pleistocene African climate.

The Arabian Sea dust record (deMenocal et al., 1991; deMenocal, 1995, 2004) is based on continuous whole-core measurements of magnetic susceptibility of sediments from ODP Sites 721 and 722, which were drilled near the crest of the Owen Ridge (Figs. 1 and 3). Magnetic susceptibility was converted to terrigenous dust percentages using a regression model calculated from a suite of magnetic and terrigenous percent measurements on selected samples. The dust record is expressed by flux of aeolian dust ($g\,cm^{-2}\,kyr^{-1}$), and is considered here back to 5 Ma. Age control for this record was provided by an oxygen-isotope stratigraphy back to 1.004 Ma (Clemens and Prell, 1991), four biostratigraphic age control points at 1.110, 1.570, 1.900 and 3.540 Ma and the Matuyama/Gauss magnetic reversal at 88.3 m composite core depth corresponding to 2.470 Ma using the chronology of Berggren et al. (1985). The transport of dust into Site 721/722 (deMenocal et al., 1991; deMenocal, 1995, 2004) mainly occurs during boreal summer, when the NW blowing *Shamal* winds lift up dust from the Arabian peninsula and transports it into the Arabian Sea over the SW Asian monsoon (deMenocal, 1995; Clemens, 1998; Prospero et al., 2002), which might also transport dust from the Horn of Africa (Fig. 1). During boreal winter, the monsoonal circulation is reversed, so the NE Asian monsoon transports moisture from the Arabian Sea into the Horn of Africa resulting in negligible dust transport (Clemens, 1998).

The eastern Mediterranean dust record (Larrasoaña et al., 2003) is based on continuous whole-core measurements of an artificially induced magnetic remanence (labelled IRM@AF) of sediments from ODP Site 967, which was drilled in the northern slope of the Eratosthenes Seamount (Figs. 1 and 4). The artificial remanence is an isothermal remanent magnetization (IRM) applied at 0.9 T that was later demagnetized using an alternating magnetic field, and reflects variations in the amount of hematite delivered as a constituent of aeolian dust. Here, we have converted IRM@AF intensities into hematite contents assuming that the IRM of hematite acquired at 0.9 T is of $\sim$0.1 Am^2/kg (Dunlop and Özdemir, 1997). We have then converted hematite contents into dust contents considering a typical hematite concentration in eastern Mediterranean dust of 6.5% in weight (Tomadini et al., 1984). The dust record extends back to 3 Ma, and is expressed by the flux of aeolian dust ($g\,cm^{-2}\,kyr^{-1}$). The age model for this record is that of Kroon et al. (1998), and was developed by tuning the characteristic sapropel pattern to an orbital precession target curve. The age model is further constrained by nannofossil datums (Staerker, 1998) and by oxygen-isotope data for the last million years, where the sapropel pattern is not as distinctive as before 1 Ma (Larrasoaña et al., 2003). Transport of dust into the eastern Mediterranean Sea mainly occurs in late winter and spring, in connection with the activity of Mediterranean depressions (Dayan et al., 1991; Goudie and Middleton, 2001) (Fig. 1). The dust is transported northward from the northeastern Sahara at the eastern side of these so-called *Sharav* cyclones, while cold, high-latitude air invades the Mediterranean basin at the western side of the fronts (Dayan et al., 1991). Throughout the rest of the year, predominant NNE-blowing winds (*Haboob*) transport dust from the northeastern Sahara into the central areas of the Sahara.

The subtropical West African dust record (Tiedemann et al., 1994) is based on the non-carbonate fraction of sediments from ODP Site 659, which was drilled on top of the Cape Verde Plateau (Figs. 1 and 5). The non-carbonate fraction is interpreted to represent terrigenous dust supply because the concentration of biogenic opal, organic carbon, volcanic glass and other terrigenous components related with fluvial and turbiditic activity is considered negligible. The dust record is expressed by flux of aeolian dust ($g\,cm^{-2}\,kyr^{-1}$), and has an astronomically calibrated isotope timescale back to 5 Ma that has been fined-tuned to the precessional cycle (Tiedemann et al., 1994). This chronology has been readjusted by Clemens (1999), who identified several hiatuses in various depths of the sediment cores. The most significant difference between the original and revised age models is the addition of a 41 kyr core break at ca 3.9 Ma (Clemens, 1999) that does affect the analysis presented here. All other readjustments are in the order of one precessional cycle or less and therefore not relevant to this study. The transport of dust to Site 659 (Tiedemann et al., 1994) is governed by seasonal variations. During boreal summer, insolation maxima over northern Africa lead to the formation of convective systems at around 18°N latitude (Fig. 1, upper panel) (Tetzlaff and Peters, 1988; Gasse, 2000). These low-pressure systems result from the low-level convergence of the moist SW monsoons and the dry NE trades, and are responsible for rainfall in the Sahel area (i.e., between the Saharan desert and the subtropical savannah). Convergence along these convective systems also result in the mobilization of dust and its injection into mid-tropospheric (2–5 km) levels, where it is transported westward into the tropical Atlantic by the *Saharan Air Layer* (SAL) (Tetzlaff and Peters, 1988; Tiedemann et al., 1994; deMenocal, 1995; Goudie and Middleton, 2001; Prospero et al., 2002). Dust uptake occurs along an E–W oriented band, which is located between 14°N and 25°N latitude, that extends from the Atlantic coast to the Chad basin and widens towards the Atlantic Ocean (Goudie and Middleton, 2001; Prospero et al., 2002). Trade winds, which undercut the SAL (Tetzlaff and Peters, 1988), also transport dust during the summer from the Mauritanian and the Western Saharan coast into the tropical Atlantic (Goudie and Middleton, 2001; Prospero et al., 2002). During boreal winter, the low-pressure systems migrate southward following increased sensible heating over subtropical southern Africa (Gasse, 2000) (Fig. 1, lower panel). Transport of dust into the tropical Atlantic is then restricted to the action of the trade winds (deMenocal, 1995). Dust produced in the Chad basin during the winter is transported into the equatorial Atlantic by the *Harmattan* (Goudie and Middleton, 2001; Prospero et al., 2002).

3. Paleoclimatic significance of the dust flux records

Dust production is related to a number of variables, among them being the most important the availability of fine-grained sediments, which fuels formation of small ($<$10 μm) dust particles, and rainfall, which enables the growth of vegetation that stabilizes surface sediments against deflation (Middleton, 1985; Prospero et al., 2002). Based on an exhaustive examination of global dust-source areas derived from Total Ozone Mapping Spectrometer (TOMS) analyses, Prospero et al. (2002) have demonstrated that most of the major dust producing areas around the globe are located in topographic lows that are characterized by (1) an arid or hyperarid climate ($<$200–250 mm annual rainfall) that results in the absence of the vegetation cover, (2) the presence of ephemeral streams that transport sediments from surrounding reliefs to terminal alluvial fans, playas and saline lakes, and (3) the evidence for recent pluvial activity, which is manifested by the presence of fluvial, alluvial, deltaic and lacustrine sediments. This paradoxical link between present-day aridity, ephemeral fluvial activity and a past pluvial history with the production of dust suggest that dust is not so much an indicator of aridity as it is of a recent transition from a relatively wet to an arid or hyperarid climate (Goudie and Middleton, 2001; Prospero et al., 2002).

The Holocene represents the last wet-arid transition in the Saharan desert, therefore it can provide the clues to evaluate the paleoclimatic significance of sedimentary dust records in peri-Saharan ocean basins during the Plio-Pleistocene. Widespread geological, paleoclimatic, paleontologic, palynological and archaeological evidence scattered throughout the whole Saharan desert demonstrates that during the early-middle Holocene period

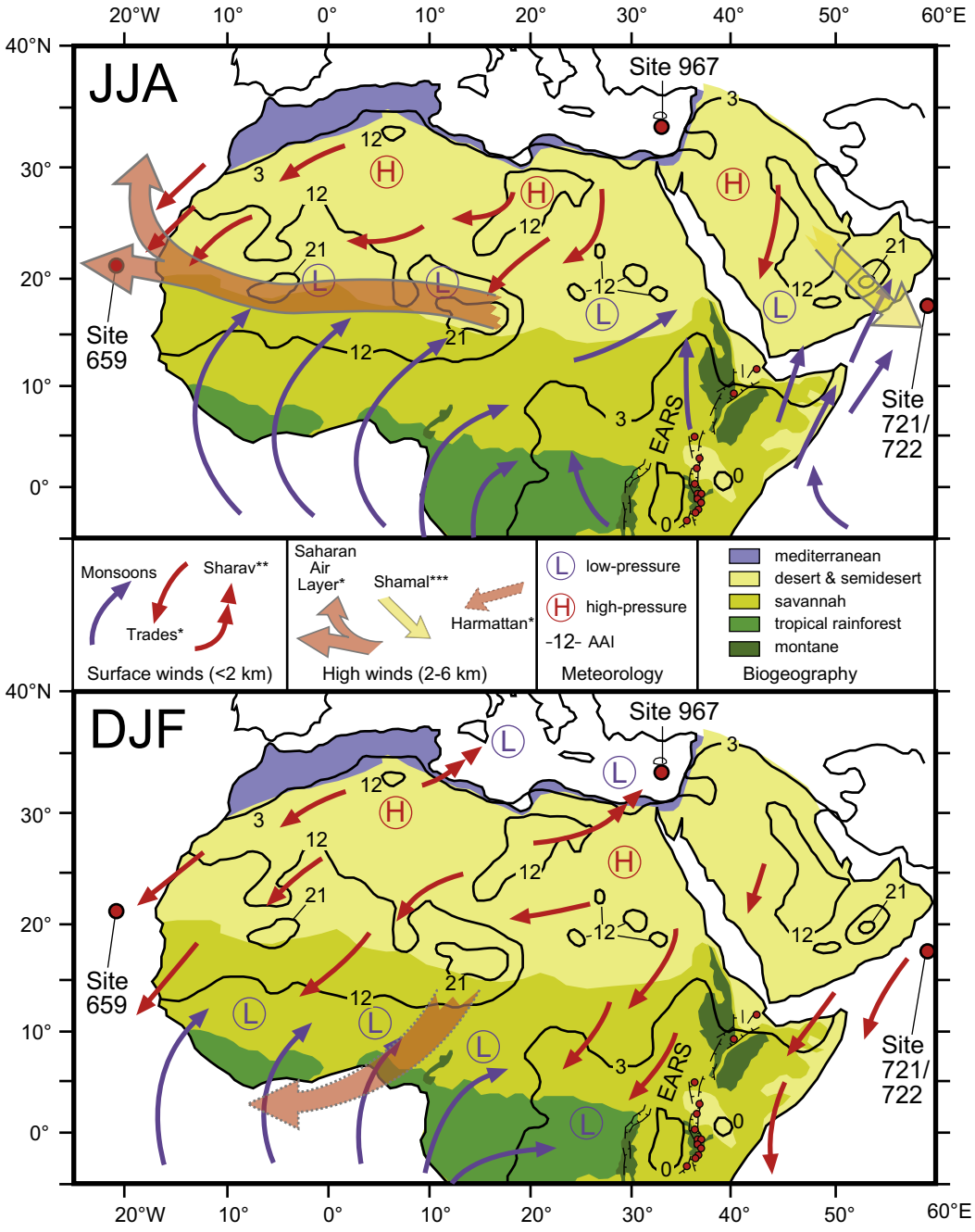

Fig. 1. Map with the location of the three studied ODP sites 659 (Tiedemann et al., 1994), 721/722 (deMenocal, 1995, 2004) and 967 (Larrasoaña et al., 2003), which shows vegetation zones (after White, 1983) and the general pattern of summer (June/July/August, upper Panel) and winter (December/January/February, lower Panel) wind and pressure systems (after Tetzlaff and Peters, 1988; Dayan et al., 1991; Tiedemann et al., 1994; deMenocal, 1995, 2004; Clemens, 1998; Gasse, 2000; Goudie and Middleton, 2001; Prospero et al., 2002) over North Africa and the Arabian peninsula. Wind systems transporting dust over the Atlantic Ocean, the Mediterranean Sea, and the Arabian Sea are marked by *, ** and ***, respectively. Height of dust-carrying winds refers to the sea surface over which the blow. Annual aerosol index (AAI) contours delineating main dust-source areas are after Goudie and Middleton (2001). Red dots mark the location of Plio-Pleistocene lake basins in the East African Rift System (EARS) studied by Trauth et al. (2005, 2007).

(ca 10–6 kyr BP), the present-day largest hyperarid desert on earth was dominated by savannah landscapes that extended as far north and east as to the Libyan desert (eastern Libya and western Egypt) (Jolly et al., 1998). Pollen, faunal and archaeological data indicate that the entire Sahara was then covered by sparsely wooded grasslands and was inhabited by savannah to semi-desert dwellers, including humans (Nicoll, 2004; Küper and Kröpelin, 2006). Moreover, the Sahara hosted fluvial networks and wetland areas, in some cases as large as present-day east African lakes at that time (Schuster et al., 2005; Armitage et al., 2007). This "greening of the Sahara" has been linked to an intensification of the West African monsoon, whose summer front shifted ~800 km northward due to positive vegetation-albedo feedbacks, in response to a maximum in boreal summer insolation, and hence in sensible heating, over the Sahara at that time (Brovkin et al., 1998; Jolly et al., 1998; Gasse, 2000). From ~7 kyr BP onwards, decreased boreal summer insolation lead to the weakening of the monsoon and the southward retreat of its summer front, which conditioned the return of hyperarid desert conditions to the Sahara (Brovkin et al., 1998; deMenocal et al., 2000; Gasse, 2000).

The "green Sahara" scenario explains the dust minimum observed for the early-middle Holocene in the tropical Atlantic

region where ODP Site 659 is located (~22°N) (deMenocal et al., 2000; Adkins et al., 2006). As the summer convective systems and the SAL increasingly shifted northwards over the course of the early-middle Holocene, they mobilized dust in desert areas located ahead of the also northward migrating desert-savannah boundary, until it eventually reached its maximum northward position at ~25°N (Gasse, 2000). This interpretation explains the paradoxical maximum in dust contents in marine records from the North Canary basin (~32°N) during the early-middle Holocene (Moreno et al., 2001; Bozzano et al., 2002; Kuhlmann et al., 2004), despite the simultaneous "green Sahara" scenario evidenced by paleoclimate and climate modeling data. The southward shift of the summer monsoon front after ~7 kyr BP, followed by a migration of the desert-savannah boundary at ~5 kyr BP (deMenocal et al., 2000; Liu et al., 2007), results in different scenarios for production and transport of dust depending on latitudinal position. In the tropical Atlantic region where ODP Site 659 is located (~22°N), dust flux experiences a marked increase at that time (deMenocal et al., 2000; Adkins et al., 2006). This increase is conditioned by the presence of early-middle Holocene fluvial and lacustrine sediments in the present-day Sahel, which fuels the production of large amounts of dust that are easily deflated, uplifted and transported into the tropical Atlantic by the convective systems and the SAL. In the North Canary basin, however, decreased dust contents (Moreno et al., 2001; Bozzano et al., 2002) attests to the southward shift of the convective systems and the SAL, which cannot transport dust into the open ocean despite of the availability of early-middle Holocene fluvial and lacustrine sediments and prevailing hyperarid conditions in the Sahara at ~25°N. This situation described for the early-middle Holocene also explains variations in dust contents back in time. Thus, "yellow Sahara" periods driven by minima in boreal summer insolation result in systematic highest dust contents in the tropical Atlantic (ODP Site 659, Tiedemann et al., 1994), but coincide systematically with lowest dust contents in the North Canary Basin (Moreno et al., 2001; Bozzano et al., 2002; Kuhlmann et al., 2004) in response to the southward migration of the summer convective systems and the SAL.

The interpretation of the Arabian Sea dust records might be more complicated than those from the Atlantic Ocean because (1) the Arabian Sea receives dust mainly from the Arabian Peninsula (Prospero et al., 2002), but might also receive dust from the Horn of Africa (Jung et al., 2004), (2) the Arabian Sea is under the influence of both the East African and the SW Asian monsoons, which might respond differently to insolation forcing (Weldeab et al., 2007), and (3) in contrast to the West African monsoon, the geographical extent of changes in vegetation cover throughout the putative dust sources, and therefore its influence on dust production is not well constrained. In any case, the production of dust in the different source areas and its transport into the Arabian Sea are both linked to monsoon dynamics, and separating the contribution of these two effects from dust flux records might be very complex. Interpretation of eastern Mediterranean dust records is simpler because, in contrast to the Atlantic Ocean and Arabian Sea, the mechanisms that control the transport of dust and those that modulate dust production are genetically unrelated. Thus, the activity of Mediterranean depressions, which transport dust from the northeastern Sahara in late winter and spring, is independent from West African monsoon dynamics, which modulates dust production within the Sahara through the "greening of the Sahara" mechanism. For this reason, ODP Site 967 shows a marked decrease in dust flux during the early-middle Holocene in response to damped dust production in the northeastern Sahara under a "green Sahara" scenario (Larrasoaña et al., 2003), despite of a simultaneous increase in activity of the Mediterranean depressions (Duplessy et al., 2005).

4. Statistical methods to detect trends, rhythms and events

The statistical analysis of dust records provides a fundamental source of information about the trends, rhythms and events in Plio-Pleistocene African climate change. We analyzed the three representative long dust records from the eastern subtropical Atlantic Ocean, eastern Mediterranean Sea and Arabian Sea for significant trends in central tendency and dispersion, significant orbital cycles, and the transitions in the eccentricity, obliquity and precession frequency bands. The identical suite of algorithms is used to analyze the ODP 659 benthic oxygen-isotope record.

The long-term trends in paleoclimate time series are usually mapped using a *classical linear regression analysis*. Classical regression, however, is based on the assumption of a normal distribution in the deviations of the observed values from the regression line. If the distribution of errors is asymmetric or prone to outliers, model assumptions are invalidated, and parameter estimates, confidence intervals, and other computed statistics become unreliable. *Robust regression* as an alternative to classical regression implements a robust fitting method that is less sensitive than ordinary least squares to large changes in small parts of the data (Holland and Welsch, 1977). We also applied a new parametric, nonlinear regression technique called "breakfit regression" to quantify trends that allow for change points (Mudelsee, in preparation). The "break model" is a continuous, but not necessarily differentiable function consisting of two linear parts that are joined at time $t2$. The break model can be fitted to data using a weighted least-squares criterion combined with a brute-force search for $t2$. A similar model ('ramp'), consisting of three parts, has been previously introduced (Mudelsee, 2000). The statistical uncertainties of the break model parameters, in particular of $t2$, were determined using 400 block bootstrap simulations (Künsch, 1989). The block bootstrap preserves distributional shape and serial dependence over the length of a block. Higher autocorrelation in the time series requires to use a larger block length (Carlstein, 1986). For details on bootstrap resampling in regression problems and numerical techniques, see Mudelsee (2000). All $t2$ estimates are given with standard error; note that the standard errors are 1.4826 times *MAD*, where *MAD* is the median of absolute distances to the median. That is, this standard error is a robust version of the standard deviation.

A number of methods are available to detect more abrupt changes in paleoclimate records in the time domain, e.g. the *rampfit method* (Mudelsee and Stattegger, 1997; Mudelsee, 2000) and in the frequency domain, e.g., evolutionary *Blackman-Tukey powerspectrum* and *Wavelet powerspectrum* (e.g., Lau and Weng, 1995; Mackenzie et al., 2001). In most cases, trends and events in the time and frequency domain are detected by computing the statistical parameters of the data (e.g., measures of central tendency and dispersion) contained in a sliding window of length L. The precision of these parameters depends on the length of the window, i.e., an accurate value for the mean and the variance is obtained if L is large. On the other hand, a larger window reduces the accuracy of the estimate for a change in these parameters. This problem is often described as *Grenander's uncertainty principle of statistics* (Grenander, 1958). Performing a statistical test to assess the difference in the central tendency and dispersion of the data contained in a paired sliding window, however, partly overcomes this problem if only the knowledge of the location of a sharp transition in statistical parameters is required.

The classic t- and F-test statistic are often used to compare means and variances of two sets of measurements and could therefore be used to detect shifts in the location and dispersion between two sliding windows. These two tests, however, make the basic assumption that these samples were collected from

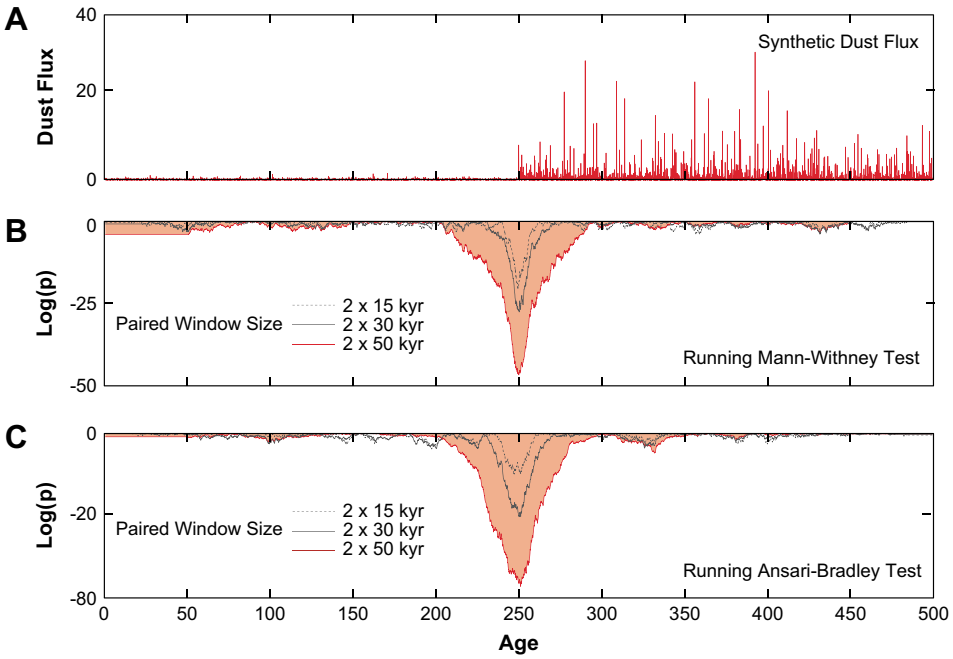

Fig. 2. Running Mann–Whitney and Ansari–Bradley tests of synthetic dust flux record. (A) Log-normal distributed noise. After 250 kyr the mean and variance of the data shifts towards a lower value. (B) Result of a running Mann–Whitney test for three different lengths of the paired sliding windows (150, 250 and 500 data points, equivalent to 15, 25 and 50 kyr). The length of the window clearly influences the amplitude and width of the maxima of the parameter, whereas the location of the transition in the means is well defined. (C) Result of a running Ansari–Bradley test for three different lengths of the paired sliding windows (150, 250 and 500 data points, equivalent to 15, 25 and 50 kyr). The length of the window clearly influences the amplitude and width of the maxima of the parameter, whereas the location of the transition in the dispersion is well defined.

a Gaussian distribution. At least the dust records, however, clearly show a significant positive skewness since they have a lower limit of zero and a large dispersion. The non-parametric *Mann–Whitney* and *Ansari–Bradley* tests, however, provide a more elegant solution to the problem independent from the distribution that is being used. The *Mann–Whitney U-test* (also called the *Wilcoxon or Mann–Whitney–Wilcoxon test*; Mann and Whitney, 1947; Lepage, 1971) performs a two-sided rank sum test of the null hypothesis that two samples come from identical continuous distributions with equal medians, against the alternative that they do not have equal medians. The *Ansari–Bradley test* performs a two-sided test that two independent samples come from the same distribution, against the alternative that they come from distributions that have the same median and shape but different dispersions (Ansari and Bradley, 1960; Lepage, 1971).

We first demonstrate the performance of the running Mann–Whitney and Ansari–Bradley test on two synthetic dust records with significant shifts in the measures of central tendency (mean, median, and mode) and dispersion (range, variance, and quantiles) in the middle of the time series (Fig. 2). The time axis runs from 0.1 to 500 kyr with 0.1 kyr intervals. At 250 kyr the mean of the log-normal distributed data shifts from initially 1.0 to a value of 1.3 and the variance changes from 0.5 to 1.3 (Fig. 2, Panel A). The result of a running Mann–Whitney test for three different lengths of the paired sliding windows (150, 250 and 500 data points, equivalent to 15, 25 and 50 kyr) reveals that the length of the window influences the amplitude and width of the maxima of the test parameter, whereas the location of the transition in the means is well defined (Fig. 2, Panel B). Fig. 2, Panel C shows the result of a running Ansari–Bradley test for three different lengths of the paired sliding windows (150, 250 and 500 data points, equivalent to 15, 25 and 50 kyr). The length of the window clearly influences the amplitude and width of the maxima of the test parameter, whereas the location of the transition in the dispersion is well defined.

5. Results

We apply the running Mann–Whitney and Ansari–Bradley tests to some of the established records of environmental change. First, we analyze the terrigenous dust flux (in $g\,cm^{-2}\,kyr^{-1}$) of ODP Site 721/722 from the Arabian Sea available for download from the author's webpage (deMenocal et al., 1991; deMenocal, 1995, 2004) (Fig. 3). The astronomically tuned record contains 2958 data points, the time axis runs from 6.35 to 5414.40 kyr, therefore the average spacing of subsequent data points is ca 1.83 kyr. The dust record shows a very weak, but significant linear trend of $+3.6 \times 10^{-5}\,g\,cm^{-2}\,kyr^{-2}$, assuming that the time axis runs from past to present. The absolute increase of the dust flux values amounts to $0.17\,g\,cm^{-2}\,kyr^{-1}$ or 21% of the range of detrended data during the past five million years. However, most of this increase is attributed to high dust values occurring during the last two million years of the record. Breakfit regression detects a change point in the dust record at 1.86 ± 0.44 Ma (robust 1-sigma error) indicating a stronger increase in the dust flux values after this event.

We resample the data set upon an evenly spaced time axis running from 8 to 5000 kyr in 2 kyr intervals using a linear interpolation technique. The running Mann–Whitney and Ansari–Bradley tests are computed for two adjacent sliding windows of the size $L = 100$ data points equivalent to 200 kyr each (Fig. 3, Panel B). The plot of the Mann–Whitney test statistic clearly marks the most significant transitions in the original data (Fig. 3, Panels A and B). The most significant changes in the record occur at 3.35 and 3.15 Ma marking the onset and termination of a period of significantly reduced dust flux. A less pronounced, but also significant episode of reduced dust flux occurs between 2.95 and ca 2.75 Ma, also marked in the running Mann–Whitney test. The record shows a number of less pronounced transitions, e.g., at ca 3.95, 3.70, 2.25, 2.05, 1.05, 0.90 and 0.40 Ma. This analysis reveals that the record shows a number of major and minor transitions towards a higher or lower dust flux. Our results, however, do not support the

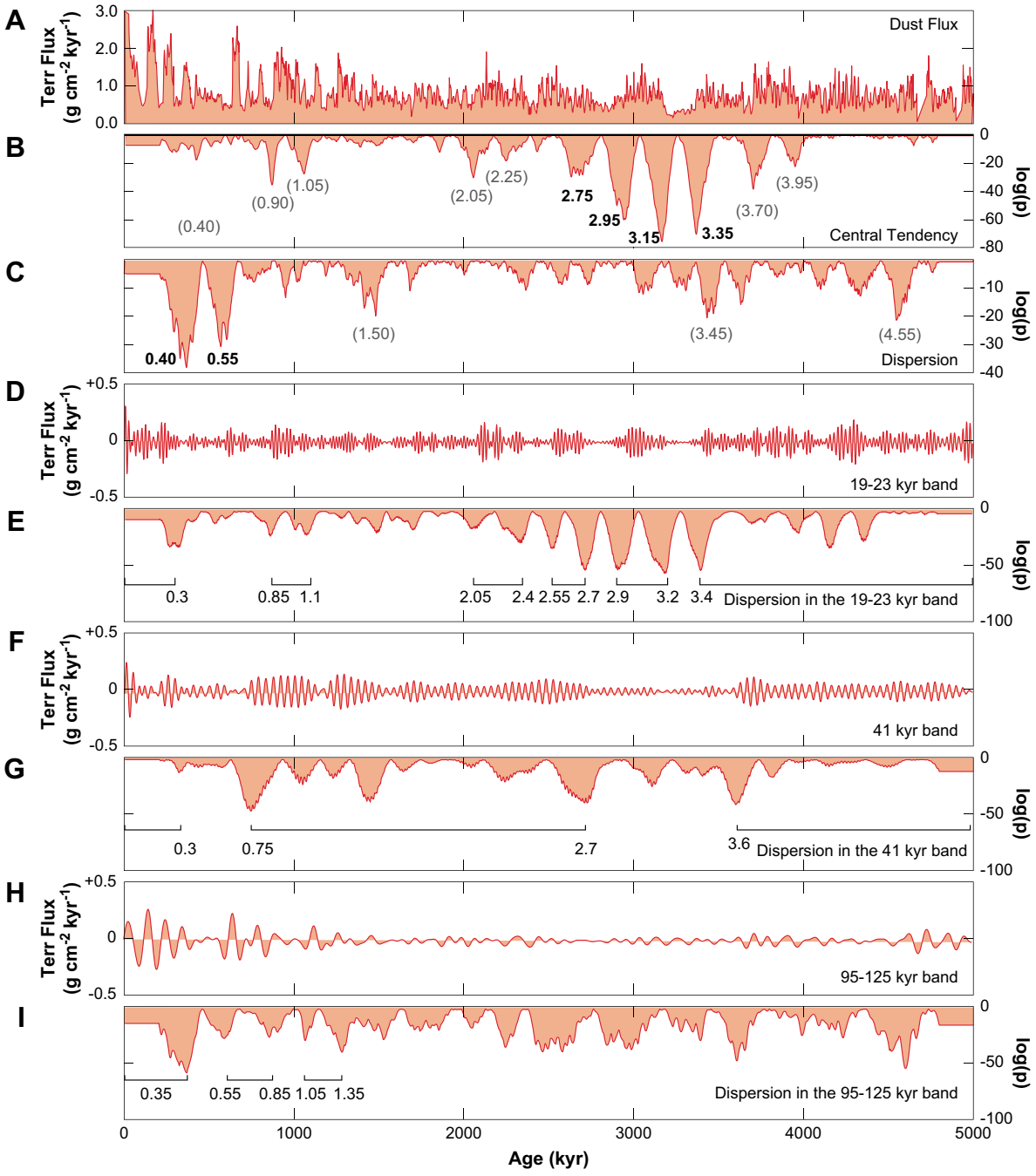

Fig. 3. (A–C) Significant shifts in the central tendency and dispersion of the dust flux record as detected by running Mann–Whitney and Ansari–Bradley tests. (A) Terrigenous dust records from ODP 721/722 (deMenocal et al., 1991; deMenocal, 1995, 2004). (B) Result from running Mann–Whitney test to detect significant shifts in the dust flux. (C) Results from running Ansari–Bradley test to detect significant chances in the dispersion of the dust flux. (D–I) Results from the event analysis of bandpass-filtered dust records from ODP 721/722 using running Ansari–Bradley test.

conclusions of the author that the record is characterized by three major shifts towards a higher dust flux at 2.8 (±0.2) Ma, 1.7 (±0.1) Ma, and 1.0 (±0.2) Ma (deMenocal, 1995, 2004).

The running Ansari–Bradley test was employed to detect major transitions in the dust variability. Fig. 3, Panel C clearly shows several weak transitions in the variability of the dust flux before 0.7 Ma, but significant changes at ca 0.55 Ma, and 0.4 Ma. Minor transitions occur at ca 4.55, 3.45 and 1.5 Ma. The Ansari–Bradley statistical analysis of the bandpass-filtered records reveal significant transitions in the Milankovitch frequency bands (Fig. 3, Panels D–I). In the 20 kyr frequency band, a series of significant transitions separate episodes of higher variability before ca 3.4, between 3.2 and 2.9, 2.7 and 2.55, 2.4 and 2.05, 1.1 and 0.85 and after ca 0.3 Ma. In the 40 kyr frequency band, a higher variability can be observed before 3.6, between 2.7 and 0.75 with an increase after 1.45, and after 0.3 Ma. The variability in the 100 kyr frequency band is generally low, with three episodes of higher variability between 1.3 and 1.05, 0.85 and 0.55, and after 0.35 Ma. This analysis reveals that the record shows a number of major and minor transitions towards an increased or reduced variability in the dust record. Our results, however, do not support the conclusions of deMenocal (1995, 2004) that the record shows three major shifts towards a higher variability at 2.8 (±0.2) Ma, 1.7 (±0.1) Ma, and 1.0 (±0.2) Ma.

The visual inspection of the other records from subtropical West Africa (ODP Sites 659, 661–664) presented by deMenocal (1995, 2004) also do not support the conclusions by the author. The

records of Sites 659 and 661, similar to 721/722 only show a very weak positive trend towards higher values during the last 4.5 Ma. These records do not show any significant transitions in the measures of central tendency or dispersion. The record of Site 664 shows a relatively abrupt transition towards higher values at ca 3.2 Ma, whereas a similar transition occurs at ca 2.85 Ma in the record of Site 664. The author does not explain the difference of 0.35 Ma in the timing of this transition, and why these transitions do not occur in the other records. The record of Site 664 also shows a transition at ca 1.2 Ma, which is not obvious in any other record. In an earlier publication on these records, deMenocal et al. (1991) proposed a shift in the mode of dust deposition at 2.4 Ma. The authors present four powerspectra integrating over the 0.1–1.0 Ma, 1.0–1.6 Ma, 1.6–2.5 Ma, and 2.5–3.2 Ma intervals. According to this publication, the record varies almost purely at 23–19 kyr periodicities between 3.2 and 2.4 Ma. A strong precession cycle is observed also after 2.4 Ma, but there is a significant increase in the variability at the 41 kyr periodicity after 2.4 Ma. The graphs presented by the authors do not show this shift in the 41 kyr frequency band. Instead, the amplitude of the precessional cycle relative to the obliquity cycle decreases with time, with a return of a slightly stronger precessional cycle in the 0–1.0 Ma interval, but not reaching the amplitude of the obliquity cycle. Our results according to the more detailed running Ansari–Bradley test analysis does not support this interpretation of the ODP 721/722 record.

Next, we apply the same approach to analyze the Eastern Mediterranean dust record from ODP 967 published by Larrasoaña et al. (2003). This tuned record contains 8417 dust flux data between 268.9 kyr and 3028.0 kyr in 359.8 ± 313.4 yr intervals. The dust record shows significant linear trend of $+3.6 \times 10^{-5}$ g cm^{-2} kyr^{-2}. The absolute increase of the dust flux values amounts to 0.17 g cm^{-2} kyr^{-1} or 24% of the range of detrended data during the past three million years. Breakfit regression detects a change point in the dust record at 1.44 ± 0.20 Ma (robust 1-sigma error) indicating a stronger increase in the dust flux values after this event.

We interpolate this data set upon an evenly spaced time axis running from 8 to 3000 kyr in 2 kyr intervals using a linear interpolation technique. We also apply the running Mann–Whitney and Ansari–Bradley tests to the full record and also to the 20, 40 and 100 kyr frequency bands (Fig. 4, Panels B + C). The Mann–Whitney test reveals a number of significant transitions, e.g., near 2.55, 2.35, 2.20, 1.95, 1.70, 1.30, 1.1, 0.95, 0.7 and 0.45 Ma, among many others (Fig. 4, Panel B). The transition at 2.55 Ma terminates a longer period of reduced dust flux values, whereas the transitions at 1.9 and 1.7 Ma bracket a second episode of lower dust values. Also, at around 1.0 Ma, a period of reduced dust flux is observed, followed by a strong increase in the dust values at ca 0.95 Ma. After ca 0.2 Ma, the dust values are significantly increased. The variability of the dust flux data shows a step-wise increase at ca 0.9 and at ca 0.2 Ma (Fig. 4, Panel C). In the 20 kyr frequency band, higher amplitudes can be observed before 2.6, between 2.25 and 1.9, 1.5 and 1.4, 1.2 and 0.5 (in particular between 0.95 and 0.8 Ma), and after 0.35 Ma (Fig. 4, Panels D–I). The 40 kyr frequency band shows higher amplitudes between 2.9 and 2.0, 1.7 and 1.0, 0.8 and 0.6 and after 0.4 Ma. The amplitude of the 100 kyr cycle is generally very low. Episodes of larger amplitudes occur between 1.9 and 1.7, 1.25 and 0.8, and after 0.6 Ma.

The next example under investigation is the ODP 659 dust record off West Africa published by Tiedemann et al. (1994). The dust flux record is tuned to the precessional cycle and contains 1236 data points between 1.96 and 5231.81 kyr in 4.22 ± 2.92 kyr intervals. The dust record shows a very weak, but significant linear trend of $+10.0 \times 10^{-5}$ g cm^{-2} kyr^{-2}. The absolute increase of the dust flux values amounts to 0.51 g cm^{-2} kyr^{-1} or 18% of the range of detrended data during the past five million years. Breakfit regression detects a change point in the dust record at 1.62 ± 0.82 Ma (robust 1-sigma error) indicating a stronger increase in the dust flux values after this event.

We again interpolated the record upon an evenly spaced time axis running from 8 to 5000 kyr in 2 kyr intervals knowing that we then increase the number of data points by a factor of two. However, this is the best solution between significantly reducing the resolution of the ODP 967 record and increasing the resolution of this record. The running Mann–Whitney test of a paired 200 kyr sliding window reveals a number of significant transitions, in particular at 4.4 Ma, among many others (Fig. 5, Panel B). The running Ansari–Bradley test also shows numerous transitions in the variability of the record, for instance a transition from higher to lower variability at ca 3.7 Ma after, a gradual increase of the variability until 3.0 Ma, a return to lower values after 3.0 Ma and again higher values after 2.8 Ma (Fig. 5, Panel C). A significant shift towards higher values can also be observed after 1.5 Ma.

The running Ansari–Bradley test indicates that the amplitude of the 41 kyr cycle indeed increases after ca 3 Ma. The true transition on 0.1 Ma timescales is at ca 2.8/2.7 Ma, besides a short interval of a reduced obliquity cycle also between 2.2 and 1.4 Ma, according to the results from the running Ansari–Bradley test. Again looking at half-million year timescales, the 19 and 23 kyr cycle indeed switches towards reduced amplitudes at ca 1.5 Ma (Fig. 5, Panels D–I). More precisely, the most significant transitions occur at 2.3 Ma towards higher values with a return to lower amplitudes after 2.0 Ma. A second interval of reduced amplitudes occurs between ca 0.8 and 0.3 Ma. The 100 kyr frequency band shows sharp transitions near 3.2 and 3.0 marking an interval of higher amplitudes, and a shift towards higher values at ca 1.6 Ma. In summary, the statistical analysis performed here validates the interpretations by Tiedemann et al. (1994), which marked the observed transitions on timescales of half million years.

Our final example is the ODP 659 benthic oxygen-isotope record also published by Tiedemann et al. (1994). The isotope record using the author's age model shows a significant linear trend of $+2.6 \times 10^{-4}$‰ kyr^{-1}. The absolute increase of the isotope values amounts to 1.34‰ or 51% of the range of detrended data during the past five million years. The isotope data are interpolated upon the same time axis as before. The running Mann–Whitney test reveals a number of significant transitions, in particular near 4.0, 3.0, 1.7 and 1.0 Ma (Fig. 6, Panel B). The running Ansari–Bradley test also shows numerous transitions in the variability of the record, for instance a transition towards higher values near 4.15, 3.3, 2.3, 1.5 and 0.5 Ma (Fig. 6, Panel C). The 20 kyr frequency band shows an increase in the amplitudes at ca 1.9 Ma, the 40 kyr frequency band gets more important after ca 3.0 Ma, whereas the 100 kyr cycles are important after ca 1.3 Ma (Fig. 6, Panels D–I).

6. Discussion

Our statistical analysis illustrates the similarities and differences in records of Plio-Pleistocene environmental changes across different timescales (Fig. 7). On timescales of 10^6 years, the dust flux records from the Arabian Sea (deMenocal, 1995, 2004), the eastern Mediterranean Sea (Larrasoaña et al., 2003) and the Atlantic Ocean (Tiedemann et al., 1994) show an increase of 21, 24 and 18% of the range of the detrended records, respectively. This trend is comparable between the three records, but is much lower than the 51% increase observed in the benthic isotope record from ODP Site 659. In the 10^6 year frequency band, however, the breakfit regression results indicate that a trend towards higher dust flux values starts (within the error bars) at ca 1.4–1.9 Ma in the three records, which then culminate with significantly higher dust fluxes from 1 Ma onwards (Fig. 7). This apparent increase in African aridity at ca 1.5 Ma and its culmination by 1 Ma matches the progressive vegetation shift from C3 (~trees and shrubs) to C4

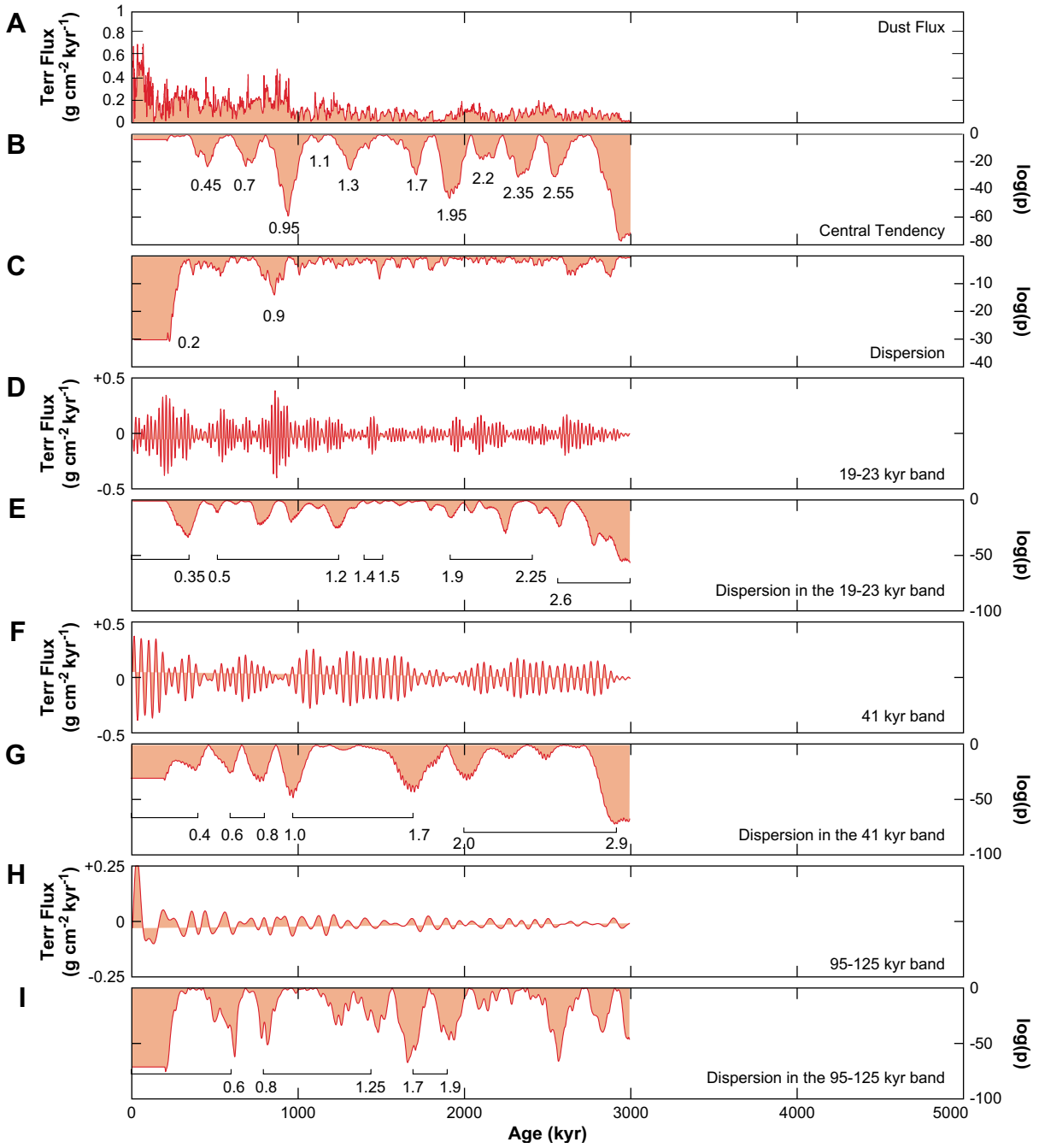

Fig. 4. (A–C) Significant shifts in the central tendency and dispersion of the dust flux record as detected by running Mann–Whitney and Ansari–Bradley tests. (A) Terrigenous dust records from ODP 967 (Larrasoaña et al., 2003). (B) Result from running Mann–Whitney test to detect significant shifts in the dust flux. (C) Results from running Ansari–Bradley test to detect significant chances in the dispersion of the dust flux. (D–I) Results from the event analysis of bandpass-filtered dust records from ODP 967 using running Ansari–Bradley test.

(~tropical grasses) plants between ca 1.5 and 0.7 Ma as derived from stable carbon isotope records (Ségalen et al., 2007). As opposed to the dust flux, oxygen-isotope values progressively increase over the full length of the record, which is marked by significant transitions in the mean and variance at the intensification of the Northern Hemisphere Glaciation (3.5–2.5 Ma, INHG) (Berger and Jansen, 1994; Mudelsee and Raymo, 2005) and the Mid-Pleistocene Transition (MPT, 1.0–0.7 Ma) (Mudelsee and Schulz, 1997; Mudelsee and Stattegger, 1997; Haug and Tiedemann, 1998; Zachos et al., 2001). This observation contradicts the hypothesis of a gradual increase in African aridity developed after the INHG (deMenocal, 2004) and suggests that African aridity responded to large ice caps only after a threshold ice volume that was attained during the MPT.

The examination of the shorter (10^4 year) frequency band reveals that precessional (19–23 kyr) and obliquity (41 kyr) forcing is continuous through most of the three dust records (Fig. 1). The ~100 kyr eccentricity band is continuously expressed through most of the ODP Site 659 record, but is evident in sites 721/722 and 967 only after ~0.8 Ma and ~1.2 Ma, respectively. These results contradict previous interpretations proposing step-like increases in the amplitude of obliquity modulation of dust fluxes at 2.8 (±0.2) Ma and 1.7 (±0.1) Ma, and also discard a common pattern of significant eccentricity modulation of dust fluxes only after 1.0

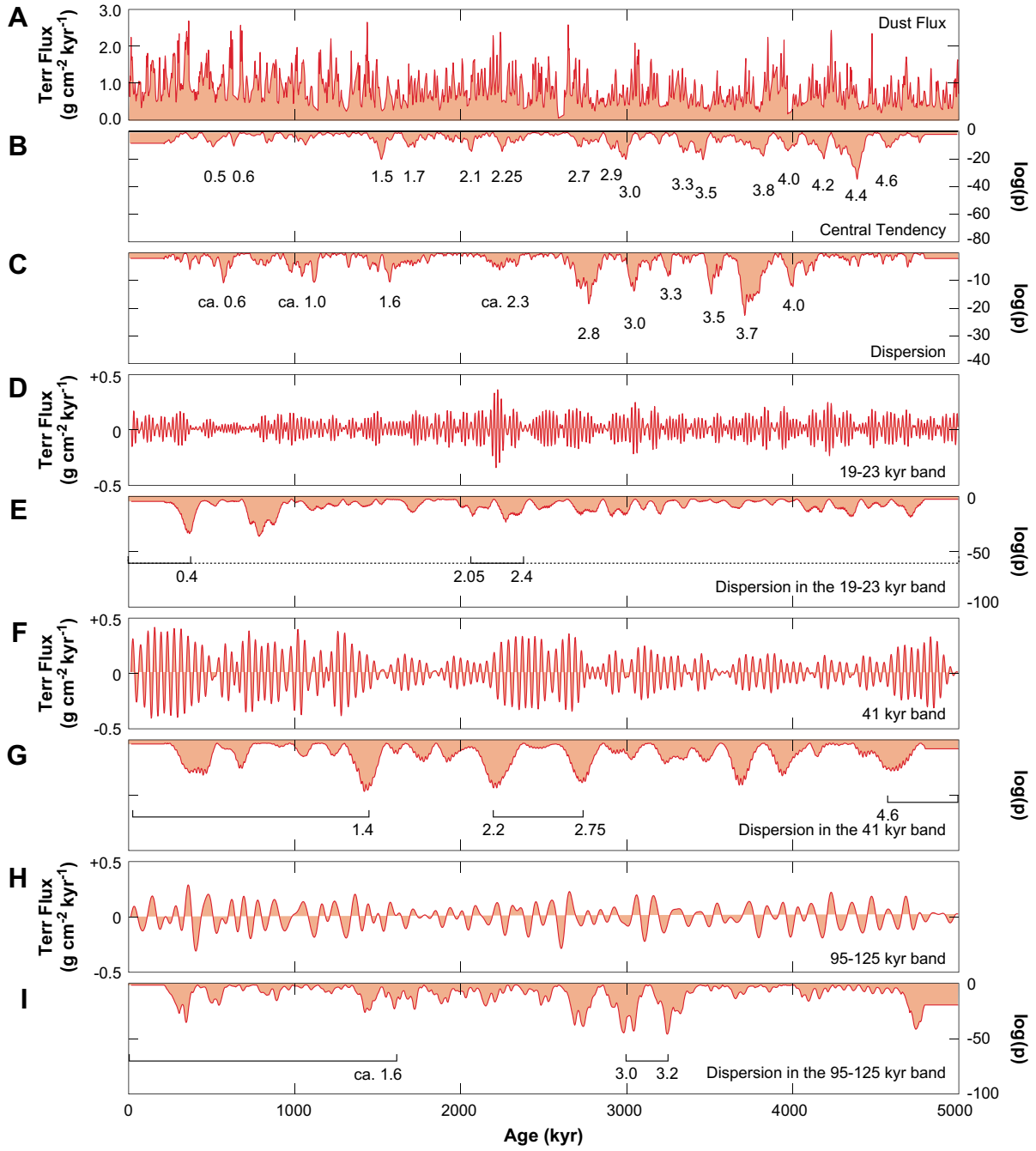

Fig. 5. (A–C) Significant shifts in the central tendency and dispersion of the dust flux record as detected by running Mann–Whitney and Ansari–Bradley tests. (A) Terrigenous dust records from ODP 659 (Tiedemann et al., 1994). (B) Result from running Mann–Whitney test to detect significant shifts in the dust flux. (C) Results from running Ansari–Bradley test to detect significant chances in the dispersion of the dust flux. (D–I) Results from the event analysis of bandpass-filtered dust records from ODP 659 using running Ansari–Bradley test.

(±0.2) Ma (deMenocal, 1995, 2004). Instead, break regression clearly indicates breakpoints in the slopes of the dust records between 1.4 and 1.9 Ma and hence after the intensification of the Walker circulation (Ravelo et al., 2004). Running Mann–Whitney and Ansari–Bradley tests detected numerous minor transitions in the amplitude and periodicity of dust flux variability in all dust records. As opposed to these results, the applications of these statistical techniques to the ODP Site 659 benthic oxygen-isotope record manifest the established shifts in the isotope values coinciding with the intensification of high-latitude glacial cycles at ca. 3.0 (near the INGP) and 1.0 Ma (near the MPT) (Tiedemann et al., 1994).

One of the most remarkable, yet unexplained, differences between the three dust flux records is that the three sites respond differently to eccentricity (95–125 kyr or ~100 kyr and 400 kyr cyclicities) (Fig. 7) (Larrasoaña et al., 2003). Highest dust fluxes correspond to ~100- and 400 kyr eccentricity minima in the eastern Mediterranean but to ~100- and 400 kyr eccentricity maxima in the Atlantic Ocean and the Arabian Sea. Interpreting this finding demands an appropriated understanding on the paleoenvironmental significance of dust flux records, which is determined by a complex interaction between the mechanisms controlling the dust production in the source areas and its transportation to the studied sites (Rea, 1994) (Fig. 7). Dust production in

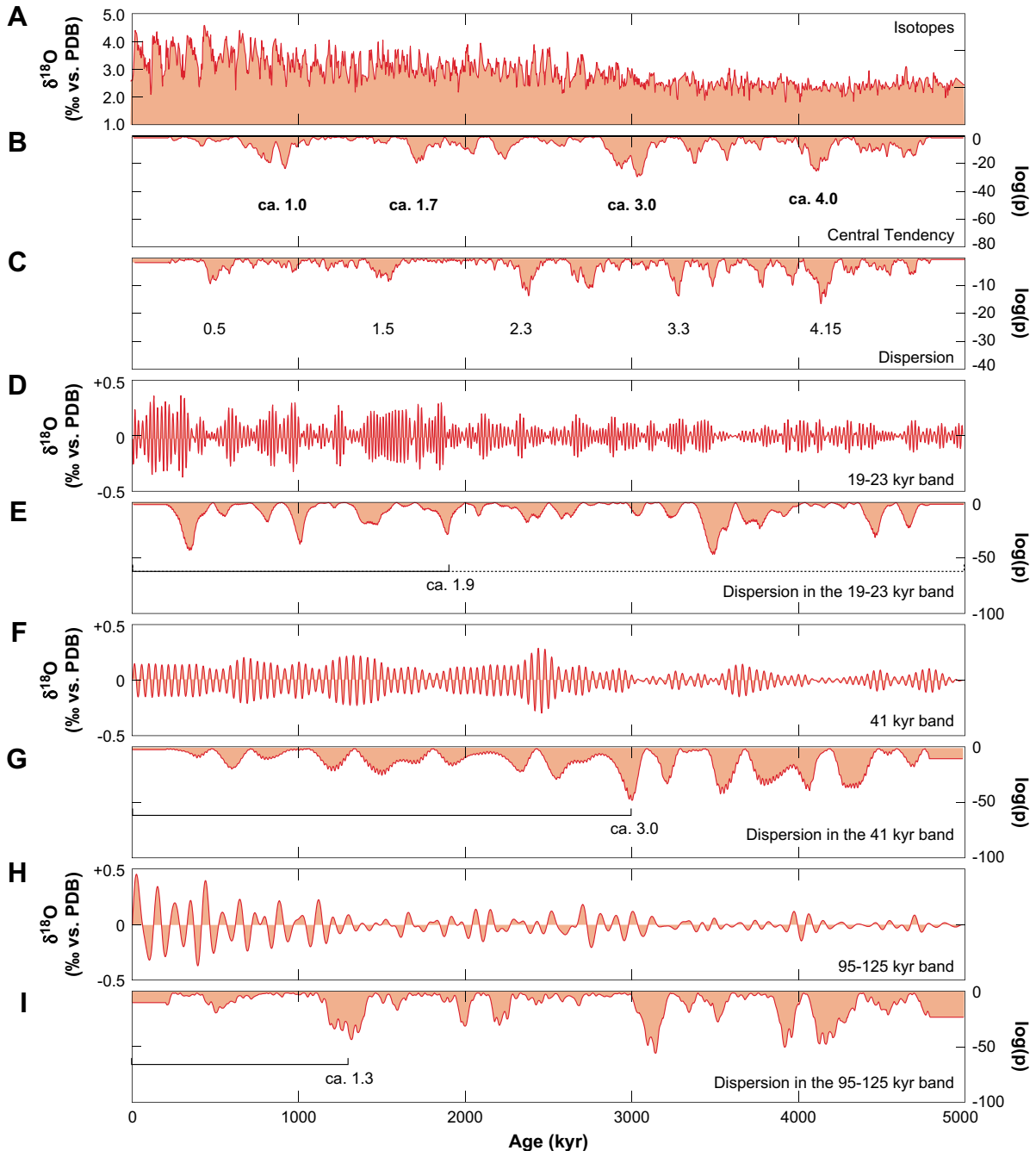

Fig. 6. (A–C) Significant shifts in the mean and variance in the benthic oxygen-isotope record as detected by running Mann–Whitney and Ansari–Bradley tests. (A) Terrigenous dust records from ODP 659 (Tiedemann et al., 1994). (B) Result from running Mann–Whitney test to detect significant shifts in the dust flux. (C) Results from running Ansari–Bradley test to detect significant chances in the variance of the dust flux. (D–I) Results from the event analysis of bandpass-filtered benthic oxygen-isotope records from ODP 659 using running Ansari–Bradley test.

the Saharo-Arabian desert belt (SADB) is suppressed during precession minima, when maxima in solar radiation over the SADB drive the "greening of the Sahara" in response to an intensification and maximum northward penetration of the African summer monsoon (Brovkin et al., 1998; deMenocal et al., 2000; Gasse, 2000). Simultaneously, monsoonal wind circulation is enhanced due to increased ocean-continent pressure gradients (Kutzbach and Street-Perrott, 1985). Due to the modulation of precession by eccentricity, the amplitude of insolation peaks during eccentricity minima is lowest and, as a result, the intensity and northward penetration of the summer monsoon front is severely diminished (Kutzbach and Street-Perrott, 1985; Gasse, 2000; Berger et al., 2006). Under these conditions, the insolation-driven "greening of the Sahara" is inactive for long ($\sim$100 and 400 kyr) periods of time, which results in high dust production in the SADB under arid to hyperarid conditions. Saharan dust is transported into the eastern Mediterranean Sea by winter–spring depressions, whose activity is independent of monsoon dynamics, and into the Atlantic and Indian oceans by summer monsoon-related winds. High dust production during $\sim$100 and 400 kyr eccentricity minima is reflected in relative dust flux maxima at ODP Site 967. Simultaneous low dust fluxes recorded at sites 659 and 721/722 likely respond to a weakened monsoon circulation, and a concomitant decrease in dust transport, despite of increased dust production throughout the SADB. During periods of eccentricity maxima (highest amplitude of insolation maxima), recurrent "green Sahara"

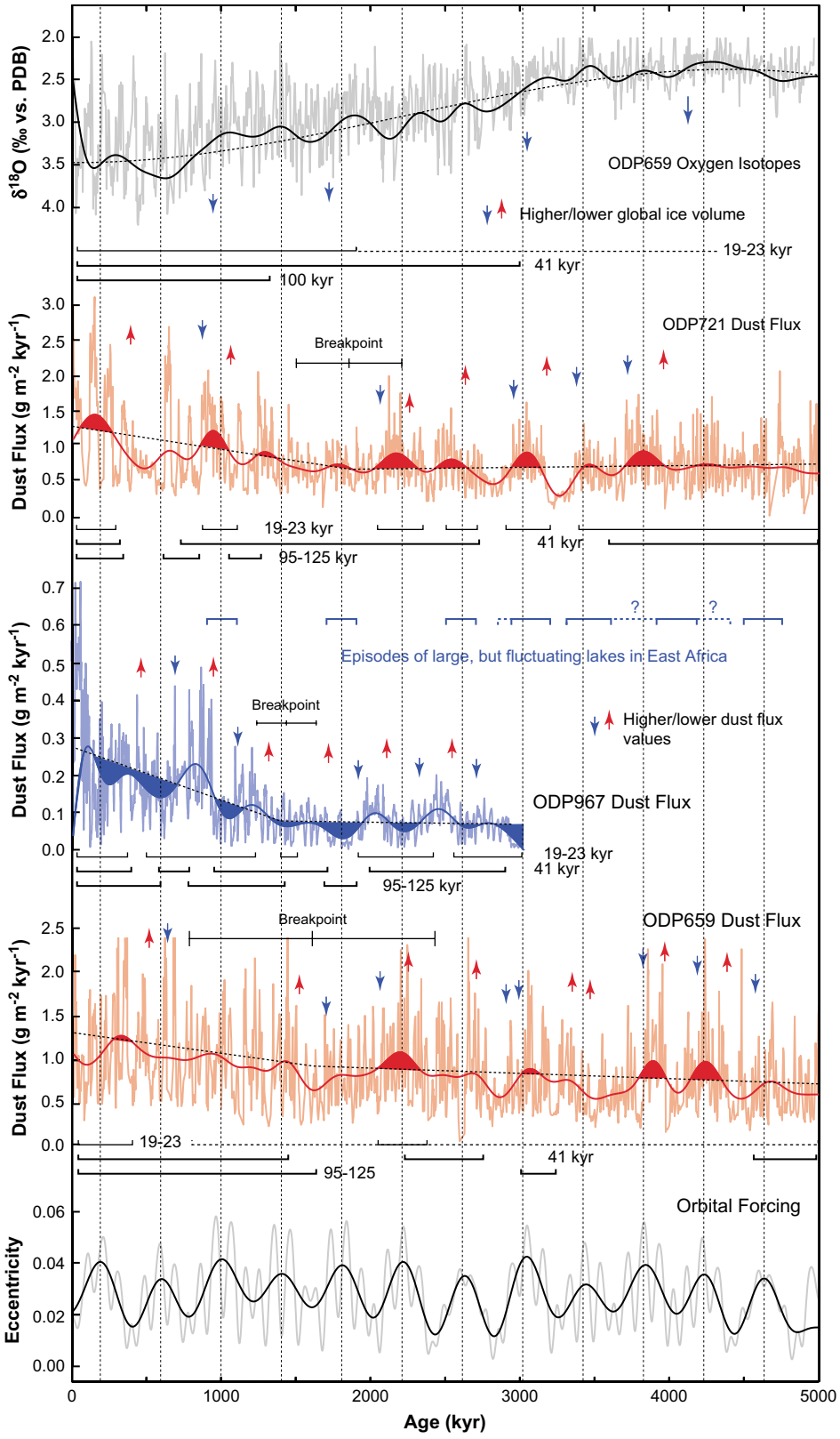

Fig. 7. Trends, rhythms and events in Plio-Pleistocene African climate based on the results of the statistical analysis. Whereas the dust flux records of ODP sites 659 (Tiedemann et al., 1994) and 721/722 (deMenocal, 1995, 2004) are overprinted by dust transport mechanism effects, the Site 967 dust flux record (Larrasoaña et al., 2003) is the only long marine record that provides a pristine view on wet/arid cycles in the Saharo-Arabian desert belt (SADB) in response to monsoon dynamics. The Site 967 dust flux correlates with Plio-Pleistocene humidity changes as recorded by East African rift lakes (Trauth et al., 2005, 2007). All records are presented as the original data series published by deMenocal et al. (1991), Tiedemann et al. (1994), deMenocal (1995, 2004) and Larrasoaña et al. (2003) and a lowpass (>350 kyr) filtered version of these data to elucidate the relation between dust flux variations and the long-term (400 kyr) component of the eccentricity cycle (Laskar et al., 2004). Breakfit regression indicates significant breakpoints $t2$ in the trends in the dust values at 1.86 ± 0.44 Ma (ODP 721/722 dust flux record), 1.44 ± 0.20 Ma (ODP 967 dust flux record) and 1.62 ± 0.82 Ma (ODP 659 dust flux record). All dust records show an increase in the trends and agree in their change point time within the error bars. The ODP 659 oxygen-isotope record is characterized by multiple breakpoints and was therefore described by a polynomial of third degree. Running Mann–Whitney and Ansari–Bradley tests detected numerous minor transitions in the amplitude and periodicity of dust flux variability in all dust records.

periods might result in an overall decrease in dust flux over the eastern Mediterranean Sea, but might result in a relative increase in dust flux over the Atlantic and Arabian Sea in response to enhanced monsoonal wind circulation. This interpretation implies that the dust flux records from sites 659 and 721/722 are overprinted by transport mechanism effects related to monsoon dynamics, as they are also affected by transport effects linked with glacial–interglacial climate variability (deMenocal, 2004). The Site 967 dust flux record might be also overprinted by transport mechanism effects during the last 1 Myr, when a significant increase in the amplitude of sub-Milankovitch variability is observed in parallel with the onset of large northern hemisphere ice sheets (Larrasoaña et al., 2003). In any case, it appears that the Site 967 dust flux record is significantly less affected by transport mechanism effects, which are restricted to glacial–interglacial effects in the last 1 Ma. We therefore interpret that the Site 967 dust flux record provides a more pristine view on wet/arid cycles in the SADB in response to monsoon dynamics. This view is supported by in-phase expansions and retractions of the SADB derived from pollen results from marine sediments located off northwest Africa (Hooghiemstra et al., 2006).

The critical reassessment of the environmental significance of dust flux records proposed here removes the major inconsistencies faced when contrasting marine vs. terrestrial records of African climate variability. Eccentricity minima lead to lowest-amplitude insolation peaks and weakened monsoon dynamics at the precessional timescale. This is manifested in East Africa by long-term (~100 and 400 kyr) periods with lowest (or even dried out) lake levels (Trauth et al., 2005, 2007), and by pervasive desert conditions in the SADB (Larrasoaña et al., 2003). To the contrary, eccentricity maxima lead to highest-amplitude insolation cycles with alternating strongest and weakest monsoons with precessional cyclicities. Eccentricity maxima are evidenced in the SADB by long-term (~100 and 400 kyr) periods where desert and "green Sahara" conditions alternate at precessional cycles (Larrasoaña et al., 2003), and in East Africa by long-term (100 and 400 kyr) periods where lake levels oscillate with largest (up to 280 m; Trauth et al., 2005, 2007) amplitudes at precession/half-precessional cycles (Trauth et al., 2003; Berger et al., 2006; Maslin and Christensen, 2007). Modulation of precession by eccentricity is evident in the dust flux records back to 5 Ma (Fig. 7), which reinforces the idea that the modulation of precession by eccentricity exerts a major control on the hydrological cycle in tropical Africa (Gasse, 2000; Trauth et al., 2003; Berger et al., 2006) and demonstrates that large-amplitude variations in tropical African climate are unrelated to the onset and amplification of high-latitude glacial cycles as previously suggested (deMenocal, 1995, 2004).

Our results provide a new basis for discussing the role of climate variability in human evolution, because they give novel insights into the underlying mechanism controlling tropical African climate and its impact on the extent and dynamics of habitats suitable for hominin occupation. Thus, our results indicate that the key junctures in hominin evolution are not linked with shifts towards more arid and variable conditions during the onset and amplification of high-latitude glacial cycles as typically proposed (deMenocal, 1995, 2004), but rather to periods of extreme climate variability on high moisture levels controlled largely by low-latitude solar heating (Trauth et al., 2007). Thus, the earliest members of the genus *Homo* and *Paranthropus* at ca 2.5–2.6 Ma, and the emergence of the Oldowan lithic complex at about the same time (see deMenocal, 2004; Trauth et al., 2007 and references therein) are centered around the 400 kyr eccentricity maxima at 2.6 Ma. The emergence of *Homo ergaster* and its out of Africa migration into Asia at ca 1.8–1.9 Ma, and the earliest occurrences of Acheulian technology at ca 1.7 Ma (deMenocal, 2004; Trauth et al., 2007), are also centered at a 400 kyr eccentricity maxima at 1.8 Ma. Finally, the extinction of the genus *Paranthropus* and of the species *H. ergaster* at ca 1.0–1.1 Ma (deMenocal, 2004; Trauth et al., 2007), also coincides with a 400 kyr eccentricity maxima at 1 Ma. This systematic link between extinction/speciation events, out of Africa range expansions, and development of new lithic technologies with eccentricity maxima points to the insolation-driven monsoon as the putative climate mechanism, if any, driving hominin evolution in tropical Africa. Thus, we propose that precessionally driven formation of large lakes in East Africa and simultaneous "green Sahara" periods might have favored hominin range expansions within and out of tropical Africa, and might also have provided protein-rich food essential to the evolution of hominin brains. Similarly, precessionally driven expansion of desert conditions in the SADB and simultaneous drying of East African lakes might have conditioned hominin range contractions. This might have resulted in isolated populations surviving in ecological refugia across tropical Africa, such as remaining wetland systems or mountain areas. Eccentricity-paced alternation between these precessionally driven scenarios might have pushed individual hominin populations, though natural selection, either to extinction or to reproductive isolation and speciation, and might have ultimately controlled the success or decline of their lithic technologies.

More archaeological, paleoanthropological and paleoenvironmental records from all tropical African locations where hominins lived are necessary to confirm our proposed concept of a major role of eccentricity cycles driving hominin evolution via their modulation of precession. If so, monsoon dynamics will be confirmed as the underlying mechanism driving environmental stress and hominin evolution in tropical Africa since at least the early Pliocene (Trauth et al., 2007), therefore giving support for the variability selection hypothesis of Potts (1998).

7. Conclusions

The robust statistical analysis presented here, aimed at detecting trends, rhythms and events in representative dust flux records from the subtropical Atlantic, the eastern Mediterranean Sea, and the Arabian Sea, sheds light on the significance of patterns of tropical African climate variability proposed in the literature. Our results demonstrate that neither the proposed gradual increase in African aridity developed after the INHG at 3 Ma, nor the 100 kyr modulation of dust fluxes only after 1.0 (±0.2) Ma, nor the step-like increases in the amplitude of obliquity modulation of dust fluxes at 2.8 (±0.2) Ma and 1.7 (±0.1) Ma, are statistically tenable. A comprehensive interpretation of the dust flux records in terms of landscape variability in the Saharo-Arabia desert, together with their comparison with lake, pollen and isotopic records of African climate variability, indicate that the hydrological cycle in tropical Africa is mainly controlled by low-latitude heating via its impact on monsoon dynamics. An examination of the fossil record indicates that the key junctures in hominin evolution reported nowadays at 2.6, 1.8 and 1 Ma coincide with 400 kyr eccentricity maxima, which suggests that periods with enhanced speciation and extinction events coincided with periods of maximum climate variability on high moisture levels.

Acknowledgements

This project was funded by two grants to M.T. by the German Research Foundation (DFG). J.C.L. benefits from a Ramón y Cajal contract (MEC). We thank the Government of Kenya (Research Permits MOST 13/001/30C 59/10, 59/18 and 59/22) and the University of Nairobi for research permits and support. We thank L. Dupont, C. Feibel, N. Marwan, M. Maslin, E. Odada, D. Olago, R. Potts, F. Schrenk, R. Tiedemann, M. Winklhofer, R. Zahn and the

participants of the EAGLE 2008 workshop at the University of Potsdam for inspiring discussions.

References

Adkins, J., deMenocal, P.B., Eshel, G., 2006. The "African humid period" and the record of marine upwelling from excess Th-230 in Ocean Drilling Program Hole 658C. Paleoceanography 22 Art. No. PA1206.

Ansari, A.R., Bradley, R.A., 1960. Rank-sum tests for dispersions. Annals of Mathematical Statistics 31, 1174–1189.

Armitage, S.J., Drake, N.A., Stokes, S., El-Hawat, A., Salem, M., White, K., Turner, P., McLaren, S.J., 2007. Multiple phases of north African humidity recorded in lacustrine sediments from the Fazzan basin, Ligyan Sahara. Quaternary Geochronology 2, 181–186.

Berger, A., Loutre, M.F., Melice, J.L., 2006. Equatorial insolation: from precession harmonics to eccentricity frequencies. Climate of the Past 2, 131–136.

Berger, W.H., Jansen, E., 1994. Mid-Pleistocene climate shift: the Nansen connection. Geophysical Monograph 85, 295–311.

Berggren, W.A., Kent, D.V., Flynn, J.J., Van Couvering, J.A., 1985. Cenozoic geochronology. GSA Bulletin 97, 1407–1418.

Bozzano, G., Kuhlmann, H., Alonso, B., 2002. Storminess control over African dust input to the Moroccan Atlantic margin (NW Africa) at the time of maxima boreal summer insolation: a record of the last 220 kyr. Palaeogeography, Palaeoclimatology, Palaeoecology 183, 155–168.

Brovkin, V., Claussen, M., Petoukhov, V., Ganopolski, A., 1998. On the stability of the atmosphere-vegetation system in the Sahara/Sahel region. Journal of Geophysical Research – Atmospheres 103, 31613–31624.

Carlstein, E., 1986. The use of subseries values for estimating the variance of a general statistic from a stationary sequence. The Annals of Statistics 14, 1171–1179.

Clemens, S.C., 1998. Dust response to seasonal atmospheric forcing: proxy evaluation and calibration. Paleoceanography 13, 471–490.

Clemens, S.C., 1999. An astronomical tuning strategy for Pliocene sections: implications for global-scale correlation and phase relationships. Philosophical Transactions of the Royal Society of London A 357, 1949–1973.

Clemens, S.C., Prell, W.L., 1991. One million year record of summer monsoon winds and continental aridity from the Owen Ridge (Site 722), northwest Arabian Sea. Proceedings of the ODP Scientific Results 177, 365–388.

Dayan, U., Heffter, J., Miller, J., Gutman, G., 1991. Dust intrusions into the Mediterranean basin. Journal of Applied Meteorology 30, 1185–1199.

deMenocal, P., 1995. Plio-Pleistocene African Climate. Science 270, 53–59.

deMenocal, P., Bloemendal, J., King, J., 1991. A rock-magnetic record of monsoonal dust deposition to the Arabian Sea: evidence for a shift in the mode of deposition at 2.4 Ma. Proceedings of the ODP Scientific Results 177, 389–407.

deMenocal, P., Ortiz, J., Guilderson, T., Adkins, J., Sarnthein, M., Baker, L., Yarusinsky, M., 2000. Abrupt onset and termination of the African humid period: rapid climate responses to gradual insolation forcing. Quaternary Science Reviews 19, 347–361.

deMenocal, P.B., 2004. African climate change and faunal evolution during the Pliocene–Pleistocene. Earth and Planetary Science Letters 220, 3–24.

Dunlop, D.J., Özdemir, Ö., 1997. Rock Magnetism: Fundamentals and Frontiers. Cambridge University Press, Cambridge.

Duplessy, J.C., Cortijo, E., Kallel, N., 2005. Marine records of Holocene climatic variations. Comptes Rendus Geosciences 337, 87–95.

Gasse, F., 2000. Hydrological changes in the African tropics since the Last Glacial Maximum. Quaternary Science Reviews 19, 189–211.

Goudie, A.S., Middleton, N.J., 2001. Saharan dust storms: nature and consequences. Earth-Science Reviews 56, 179–204.

Grenander, U., 1958. Bandwidth and variance in estimation of the spectrum. Journal of the Royal Statistical Society Series B 20, 152–157.

Haug, G.H., Tiedemann, R., 1998. Effect of the formation of the Isthmus of Panama on Atlantic Ocean thermohaline circulation. Nature 393, 673–676.

Holland, P.W., Welsch, R.E., 1977. Robust regression using iteratively reweighted least-squares.

Hooghiemstra, H., Lezine, A.M., Leroy, S.A.G., Dupont, L., Marret, F., 2006. Late Quaternary palynology in marine sediments: a synthesis of the understanding of pollen distribution patterns in the NW African setting. Quaternary International 148, 29–44.

Jolly, D., Harrison, S.P., Damnati, B., Bonnefille, R., 1998. Simulated climate and biomes of Africa during the late Quaternary: comparison with pollen and lake data. Quaternary Science Reviews 17, 629–657.

Jung, S.J.A., Davies, G.R., Ganssen, G.M., Kroon, D., 2004. Stepwise Holocene aridification in NE Africa deduced from dust-borne radiogenic isotope records. Earth and Planetary Science Letters 221, 27–37.

Kroon, D., Alexander, I., Little, M., Lourens, L.J., Matthewson, A., Robertson, A.H.F., Sakamoto, T., 1998. Oxygen isotope and sapropel stratigraphy in the Eastern Mediterranean during the last 3.2 million years. Proceedings of the ODP Scientific Results 160, 181–190.

Kuhlmann, H., Freudenthal, T., Helmke, P., Meggers, H., 2004. Reconstruction of local paleoceanography off NW Africa during the last 40,000 years: influence of local and regional factors on sediment accumulation. Marine Geology 207, 209–224.

Künsch, H.R., 1989. The jackknife and the bootstrap for general stationary observations. The Annals of Statistics 17, 1217–1241.

Küper, R., Kröpelin, S., 2006. Climate-controlled Holocene occupation in the Sahara: motor of Africa's evolution. Science 313, 803–807.

Kutzbach, J.E., Street-Perrott, F.A., 1985. Milkankovitch forcing of fluctuations in the level of tropical lakes from 18 to 0 kyr BP. Nature 317, 130–134.

Laskar, J., Gastineau, M., Joutel, F., Robutel, P., Levrard, B., Correia, A., 2004. A long term numerical solution for the insolation quantities of Earth. Astronomy and Astrophysics 428, 261–285.

Larrasoaña, J.C., Roberts, A.P., Rohling, E.J., Winklhofer, M., Wehausen, R., 2003. Three million years of monsoon variability over the northern Sahara. Climate Dynamics 21, 689–698.

Lau, K.M., Weng, H., 1995. Climate signal detection using wavelet transform: how to make a time series sing. Bulletin of the American Meteorological Society 76, 2391–2402.

Lepage, Y., 1971. A combination of Wilcoxon's and Ansari–Bradley's statistics. Biometrika 58, 213–271.

Liu, Z., Wang, Y., Gallimore, R., Gasse, F., Johnson, T., deMenocal, P., Adkins, J., Notaro, M., Prentice, I.C., Kutzbach, J., Jacob, R., Behling, P., Wang, L., Ong, E., 2007. Simulating the transient evolution and abrupt change over Northern Africa atmosphere–ocean–terrestrial ecosystem in the Holocene. Quaternary Science Reviews 26, 1818–1837.

Mackenzie, D., Daubechies, I., Kleppner, D., Mallat, S., Meyer, Y., Ruskai, M.B., Weiss, G., 2001. Wavelets: Seeing the Forest and the Trees. Beyond Discovery. National Academy of Sciences.

Mann, H.B., Whitney, D.R., 1947. On a test of whether one of two random variables is stochastically larger than the other. Annals of Mathematical Statistics 18, 50–60.

Maslin, M.A., Christensen, B., 2007. Tectonics, orbital forcing, global climate change, and human evolution in Africa: introduction to the African paleoclimate special volume. Journal of Human Evolution 53, 443–464.

Middleton, N.J., 1985. Effect of drought on dust production in the Sahel. Nature 316, 431–434.

Moreno, A., Targarona, J., Henderiks, J., Canals, M., Freudenthal, T., Meggers, H., 2001. Orbital forcing of dust supply to the North Canary Basin over the last 250 kyrs. Quaternary Science Reviews 20, 1327–1339.

Mudelsee, M., 2000. Ramp function regression: a tool for quantifying climate transitions. Computers and Geosciences 26, 293–307.

Mudelsee, M., Raymo, M.E., 2005. Slow dynamics of the Northern Hemisphere glaciation. Paleoceanography 20, PA4022.

Mudelsee, M., Schulz, M., 1997. The Mid-Pleistocene climate transition: onset of 100 ka cycle lags ice volume build-up by 280 ka. Earth and Planetary Science Letters 151, 117–123.

Mudelsee, M., Stattegger, M., 1997. Exploring the structure of the mid-Pleistocene revolution with advanced methods of time-series analysis. International Journal of Earth Sciences 86, 499–511.

Mudelsee, M., in preparation, Climate Time Series Analysis: Classical Statistical and Bootstrap Methods, Springer Verlag.

Nicoll, K., 2004. Recent environmental change and prehistoric human activity in Egypt and Northern Sudan. Quaternary Science Reviews 23, 561–580.

Potts, R., 1998. Environmental hypotheses of hominin evolution. Yearbook of Physical Anthropology 41, 93–136.

Prospero, J.M., Ginoux, P., Torres, O., Nicholson, S.E., Gill, T.E., 2002. Environmental characterization of global sources of atmospheric soil dust identified with the Nimbus 7 Total Ozone Mapping Spectrometer (TOMS) absorbing aerosol product. Reviews of Geophysics 40 Art. No. 1002.

Ravelo, C., Andreasen, D., Olivarez, A., Lyle, M., Wara, M., 2004. The Role of tropical and extratropical processes on Northern Hemisphere Glaciation. Nature 429, 263–267.

Rea, D.K., 1994. The paleoclimatic record provided by eolian deposition in the deep-sea – the geologic history of wind. Reviews of Geophysics 32, 159–195.

Schuster, M., Roquin, C., Duringer, P., Brunet, M., Caugy, M., Fontugne, M., Mackaye, H.T., Vignaud, P., Ghienne, J.F., 2005. Holocene lake Mega-Chad palaeoshorelines from space. Quaternary Science Reviews 24, 1821–1827.

Ségalen, L., Lee-Thorp, J.A., Cerling, T., 2007. Timing of C4 grass expansion across sub-Saharan Africa. Journal of Human Evolution 53, 549–559.

Staerker, T.S., 1998. Quantitative calcareous nannofossil biostratigraphy of Pliocene and Pleistocene sediments from the Eratosthenes Seamount region in the eastern Mediterranean. Proceedings of the ODP Scientific Results 160, 83–98.

Tetzlaff, G., Peters, M., 1988. A composite study of early summer squall lines and their environment over west Africa. Meteorology and Atmospheric Physics 38, 153–163.

Tiedemann, R., Sarnthein, M., Shackleton, N.J., 1994. Astronomical timescale for the Pliocene Atlantic d18O and dust flux records of Ocean Drilling Program site 659. Paleoceanography 9, 619–638.

Tomadini, L., Lenaz, R., Landuzzi, V., Mazzucotelli, A., Vannucci, R., 1984. Wind-blown dust over the central Mediterranean. Oceanologica Acta 7, 13–23.

Trauth, M.H., Deino, A.L., Bergner, A.G.N., Strecker, M.R., 2003. East African climate change and orbital forcing during the last 175 kyr BP. Earth and Planetary Science Letters 206, 297–313.

Trauth, M.H., Maslin, M.A., Deino, A., Bergner, A.G.N., Dühnforth, M., Strecker, M.R., 2007. High- and low-latitude forcing of Plio-Pleistocene East African climate and human evolution. Journal of Human Evolution 53, 475–486.

Trauth, M.H., Maslin, M.A., Deino, A., Strecker, M.R., 2005. Late Cenozoic moisture history of East Africa. Science 309, 2051–2053.

Weldeab, S., Lea, D.W., Schneider, R.R., Andersen, N., 2007. 155,000 years of West African monsoon and ocean thermal evolution. Science 316, 1303–1307.

White, F., 1983. Vegetation of Africa – A Descriptive Memoir to Accompany the UNESCO/AETFAT/UNSO Vegetation Map of Africa. U.N. Educational, Scientific and Cultural Organization, Paris.

Zachos, J., Pagani, M., Sloan, L., Thomas, E., Billups, K., 2001. Trends, rhythms, and aberrations in global climate 65 Ma to present. Science 292, 686–693.